HEFAT2014
10th International Conference on Heat Transfer, Fluid Mechanics and Thermodynamics
14 – 16 July 2014
Orlando, Florida

NUMERICAL SIMULATION OF MIXING AND COMBUSTION OF TURBULENT OPPOSED-JET

T. M. Abdel-Salam
College of Engineering and Technology,
East Carolina University,
Greenville, NC27858,
USA,
E-mail: abdelsalamt@ecu.edu

ABSTRACT

Fluid dynamics of opposed jets is not completely clarified as there are questions unanswered about flow stability and structure. The achievement of high efficiency combustion requires adequate mixing between the fuel and the oxidizer. In the present work, three-dimensional numerical simulations were conducted to study mixing and combustion of turbulent opposed-jets. The numerical simulations were carried out with a finite volume CFD code. Turbulence is treated with the two equation model, the k-ε model. Nozzle diameter (d) and nozzle separation (W) are kept constant and equals to 32mm. Also, different jet velocities (Uj) have been examined corresponding to Reynolds numbers of 4,500 to 12,000. Both confined and unconfined cases were simulated. Results for reacting flows of hydrogen-air flames are presented.

INTRODUCTION

Due to its simplicity in geometry, the opposed-jet flow configuration has been used extensively in the past for studying laminar flames [1–4].Turbulent mixing of jet flows in opposing jet configuration has many applications due to their favorable mixing features. Opposed jets have been used in industrial processes such as reaction injection molding, flame stabilization, mixing of fluids, and combustion of gasses [5]. The opposed jet configuration has been the subject of combustion research interest for many years [6]. Studies of opposed jet flows have spanned from laminar flames to turbulent combustion. Of prime interest are the influences of bulk strain rate and nozzle exit turbulence level on the mixing and velocity fields. When combustion is involved, the characteristics of flame properties and product formation are also of importance [5–10]. When a diffusion flame extinguishes locally because of excessive straining, the fuel and oxidizer streams feeding it are allowed to mix. After such extinction, flames can be obtained that, unlike the underlying diffusion flame, propagate with well-defined speed in the resulting partially premixed mixture, preferentially along the stoichiometric iso-surface. Depending on different parameters, they can have different structures at the propagating front, which, in turn, can propagate either to extend the flame, or to extend the quenched region. In addition, flame curvature, upstream mixture fraction gradient, and flame stretch make the propagation speed of such a structure different from that of a planar premixed flame [11]. In the current study results are presented for non-reacting and reacting jets. Numerical results are presented to examine the flowfields and the mixing of the two jets. Flow characteristics were simulated using air-air, the mixing cases were simulated with propane-air while the reacting cases were simulated using hydrogen-air.

NOMENCLATURE

d	[m]	Nozzle diameter
JR	[-]	Jet velocity ratio (left port to right port)
L	[m]	Outer wall diameter
Re	[-]	Reynolds number of the jet
U	[m/s]	Axial velocity
U_j	[m/s]	Initial jet velocity
Um	[m/s]	Maximum axial velocity
X,Y,Z	[m]	Coordinates
W	[m]	Separation distance between the jets

PHYSICAL MODEL

The basic dimensions of the physical model selected for the present study are similar to that of Weifeng et el. [12] as shown in figure 1. The flow field is produced by two opposed subsonic jets. The two jets have the same diameter “d” which is equal to 32 mm. The separation distance between the jets “W” is kept constant and equals to 32 mm. For the confined cases, the jets are paced in a bigger tube with a diameter “L” equals to 12d. The opposed jets are directed toward each other with a distance, W, which is of the order of jet diameter. Studies of mixing can be carried out with fuel in one stream and oxidizer in the other stream. Alternatively, air streams at different temperatures can be used [4].

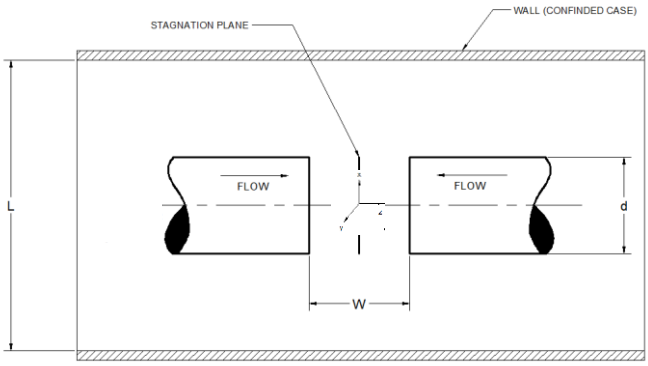

Figure 1 schematic of the physical model

MATHEMATICAL FORMULATION

Governing equations

In the present study the numerical analysis was carried out using a finite volume code for solving the Reynolds-averaged Navier-Stokes equations [13]. Reynolds averaging was used to time average the instantaneous full Navier-Stokes equations to produce Reynolds-averaged equations of fluid motion which are better suited to predict the velocity field of a turbulent flow.

Assuming the flow is steady and gravity is negligible, the incompressible form of the continuity and the momentum equations in Cartesian tensor notation are given by

$$\frac{\partial U_i}{\partial x_i} = 0 \tag{1}$$

$$\rho_{U\,j} \frac{\partial U_i}{\partial x_j} + \frac{\partial P}{\partial x_i} - \frac{\partial \tau_{ij}}{\partial x_j} = 0 \tag{2}$$

where x_i represent the Cartesian coordinates, U_i represent the Cartesian time-averaged velocity components, P represents the time-averaged pressure, and τ_{ij} is the stress tensor and is given by

$$\tau_{ij} = \left[\mu \left(\frac{\partial U_i}{\partial x_j} + \frac{\partial U_j}{\partial x_i} \right) \right] - \frac{2}{3} \mu \frac{\partial U_i}{\partial x_i} \delta_{ij} \tag{3}$$

Turbulence model

In the present study, the two-equation k-ε turbulence model is used. For this model, the Boussinesq approximation is assumed valid; it assumes that the turbulent stresses are proportional to the mean velocity gradients. Thus, specific Reynolds-stresses tensor and the turbulence kinetic energy can be calculated by the following equations [14]:

$$\tau_{ij} = 2\upsilon_t S_{ij} - \frac{2}{3} k \delta_{ij} \tag{4}$$

$$\frac{\partial k}{\partial t} + U_j \frac{\partial k}{\partial x_j} = \tau_{ij} \frac{\partial U_i}{\partial x_j} - \varepsilon + \frac{\partial}{\partial x_j} \left[(\upsilon + \upsilon_t / \sigma_k) \frac{\partial k}{\partial x_j} \right] \tag{5}$$

where ν_t is the kinematic turbulent viscosity (μ_t/ρ), S_{ij} is the mean strain-rate tensor δ_{ij} Kronecker delta, σ_k is the turbulent Prandtl number, and k is the turbulent kinetic energy. The standard k-ε model is a semi-empirical turbulent model based on model transport equation for the turbulent kinetic energy k and its dissipation rate ε [15]. The model transport equation for k is derived from the exact equation, while the model transport equation for ε is obtained using physical reasoning and bears little resemblance to its mathematically exact counterpart [10]. The turbulence kinetic energy is calculated from equation 5 and the dissipation rate is calculated from

$$\frac{\partial \varepsilon}{\partial t} + U_j \frac{\partial \varepsilon}{\partial x_j} = C_{\varepsilon 1} \frac{\varepsilon}{k} \tau_{ij} \frac{\partial U_i}{\partial x_j} - C_{\varepsilon 2} \frac{\varepsilon^2}{k} + \frac{\partial}{\partial x_j} \left[(\upsilon + \upsilon_t / \sigma_e) \frac{\partial k}{\partial x_j} \right] \tag{6}$$

where $C_{\varepsilon 1}$, $C_{\varepsilon 2}$ are constants and σ_ε is the turbulent Prandtl number.

By combining k and ε, the turbulent viscosity is calculated as

$$\nu_t = C_\mu k^2 / \varepsilon \tag{7}$$

where C_μ is a constant. The model constants have the following values [15]: $C_{\varepsilon 1}$= 1.44, $C_{\varepsilon 2}$=1.92, σ_ε= 1.3, σ_k= 1.0, and Cμ= 0.09. These default values have been determined from experiments. They have been found to work fairly well for a wide range of turbulent flows.

Chemical models:

The species transport model used for hydrogen-air is the finite rate reaction model. The model solves for each species of the four species considered (H_2, O_2, N_2, and H_2O) in the study. The reaction rate is calculated with the Magnussen model to take into account the influence of turbulence. The density, thermal conductivity, and viscosity of the hydrogen-air mixture are defined with ideal gas mixing. The specific heat capacities, thermal conductivity, and viscosity of oxygen, hydrogen, nitrogen, and water vapor are defined as polynomial.

Grids and boundary conditions

Unstructured girds are used in all cases with about 756,000 grid points. The grid nodes were reasonably distributed and arranged to ensure that regions of important influence on the flow field are adequately resolved. In general, the axial and radial grids were clustered at the nozzles exits and were concentrated within region between the two jets.

Different nozzle velocities corresponding to Reynolds number (WU/ν) of 4,500 to 12,000 are used. Uniform conditions are used for both the free stream and the jets. Initial conditions are obtained by specifying free stream conditions throughout the flowfields.

ESULTS AND DISCUSSIONS

The numerical simulations were carried out with a finite volume CFD code. Turbulence is treated with the two equation model, the k-ε model. Results are obtained for one value of nozzle diameter (d), one value of nozzle separation (W), and different jet velocities (U_j). Reynolds numbers corresponding to jet velocities are varied from 4,500 to 12,000. Before obtaining the final results, grids were examined and grid independence tests have been conducted. Results are obtained for both confined and unconfined wall conditions.

Figure 2 compares the normalized mean axial velocity magnitude with the results of Weifeng et el. [12]. The figure shows good agreement between the numerical and the experimental results.

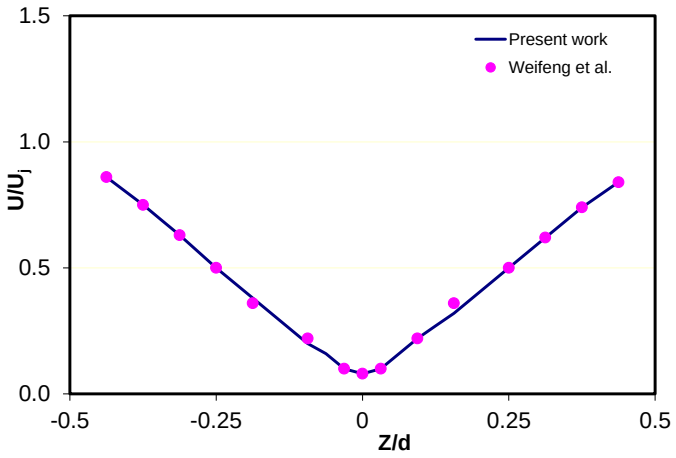

Figure 2 Comparison of the axial velocity distribution.

Opposed jets flowfield

Figures 3- 5 show velocity contour plots for Re = 8500 and 12,000 for unconfined and confined cases. Each air jet is moving with the same velocity. Jet ratio (JR) is defined the ratio of jet velocity coming from the left port to the right port. The results are shown for W/d =1 and JR =1. As shown in Figure 3, in both cases, the characteristics of opposed jets are observed. It is clear from the contour plots, a stagnation zone is formed at the center between the two jets. This is expected as the momentum of each stream is same. The stagnation zone becomes smaller for higher jet Reynolds number with increased radial component of velocity shown by the longer red zone (Re = 12,000). No recirculation zones are observed near the center. This clearly indicates the radial component of velocity stayed positive and no gas moved towards the center. Figure 5 shows the flowfields for same Reynolds numbers (8500 & 12,000; JR =1) as in the case of Figure 3 but for case of confined walls.

The wall boundary is placed at a distance of 6 d from the horizontal center plane It is clear from the velocity contour plots, the flowfields are affected by presence of the wall. The impingement zone becomes wider due to the wall effect. At Re

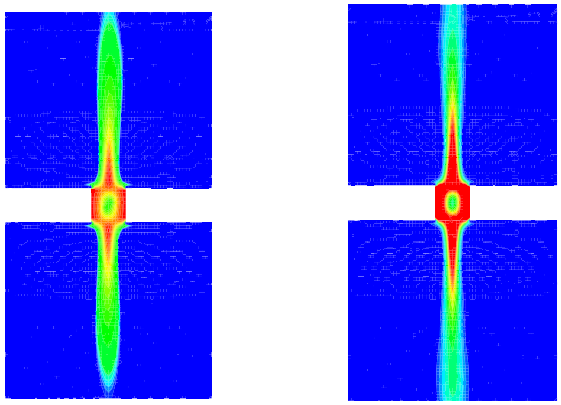

Figure 3 Velocity Contour Plots for W/d =1 & JR=1.

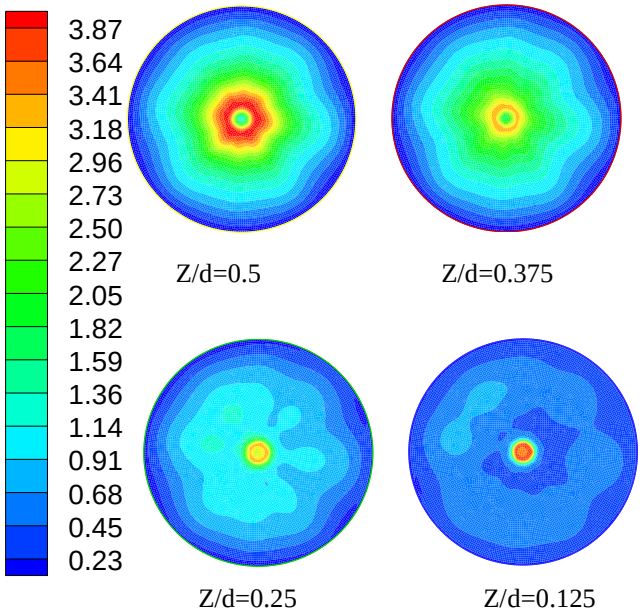

Figure 4 Velocity Contour Plots for JR=1 and different Z/d ratios.

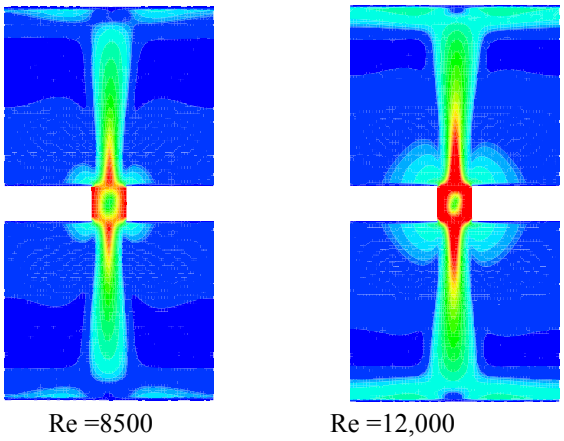

Figure 5 Velocity Contour Plots for W/d =1 & JR=1 (Confined)

=12,000 impingement zone hits the wall and splits into two equal halves.

Opposed jets mixing

Figure 6 shows the spread of the propane jet at different locations from the exit nozzle. Figure7 shows line and flooded contour plots of mole fraction of propane for unconfined boundary condition. Propane is injected from left to right. The jet ratio is equal to 1. Even though propane and air are moving at the same velocity, the flow is curving towards right. This is because the momentum of propane jet is higher than that of air due to its high density as compared to that of air. The mole fraction of propane is decreasing away from the stagnation zone, indicating mixing with air. Figure 8 shows the mole fraction contour line plots for confined boundary condition. As in the case of air-air, the flow fields are affected by the boundary for the JR =1.

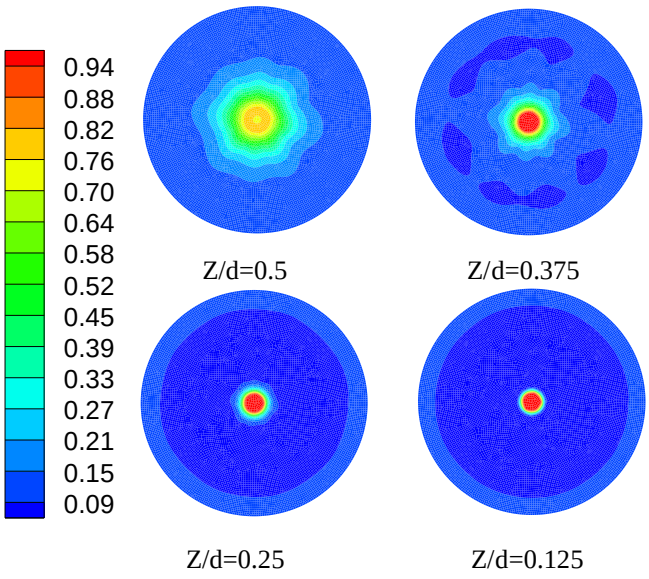

Figure 6 Cross contours of the mole fraction of propane.

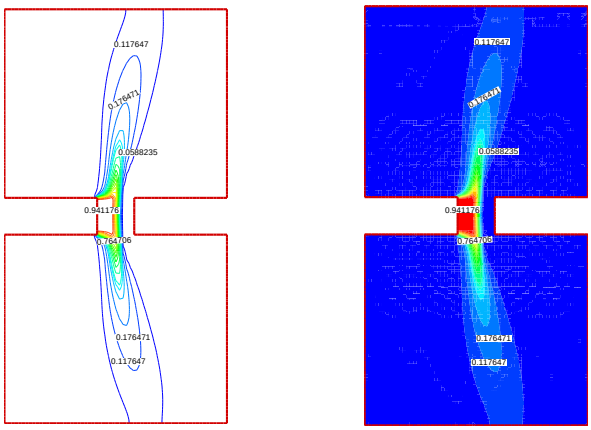

Figure 7 Line and Contour Plots of propane mole fraction for W/d =1, JR=1, Re = 8500 (3-D, Unconfined)

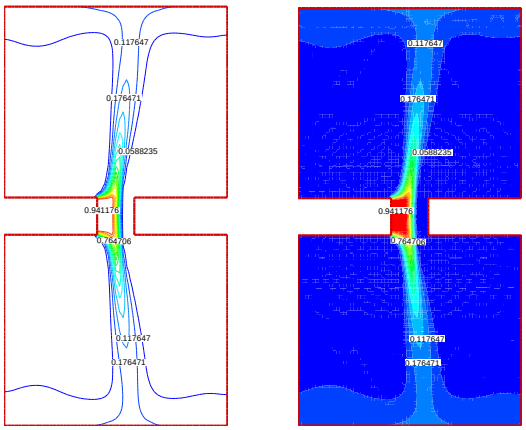

Figure 8 Line and Contour Plots of propane mole fraction for W/d=1, JR=1, Re = 8500 (3-D, Confined)

One of the methods that have been used to express the mixing rate of the fuel and the air is the decay of the maximum mole fraction downstream of the nozzle. Figure 9 shows variation of maximum mole fraction with Z/d for unconfined boundary condition. It is seen that the maximum mole fraction decreased from 1 (no mixing) to less than 80 percent of its maximum value approximately at the stagnation plane (Z/d=0). Mole fraction is continuously decaying to a value of about 15 percent of its maximum value at Z/d=0.5 indicating mixing of propane with air for all values of Re.

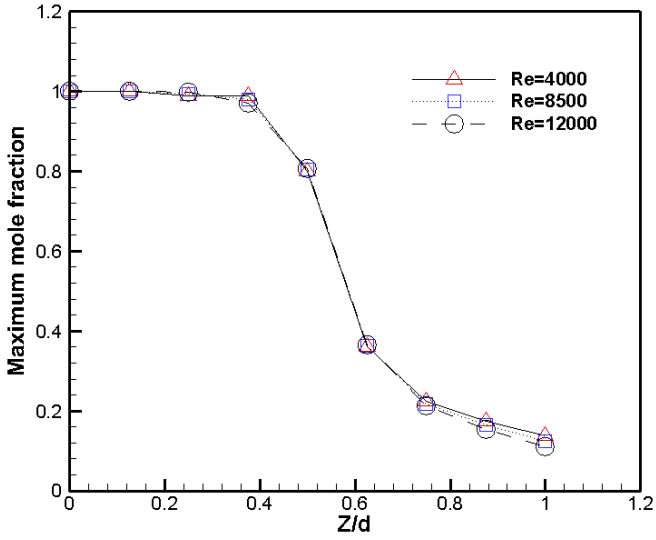

Figure 9 Decay of the maximum mole fraction for different values of Re.

Reacting flow

Results for the reacting flow are presented in this section. in all cases, the input oxidizer is 21% O_2 and 79 % N_2 by volume whereas the main fuel is 100% hydrogen. Figure 10 shows iso-contours of water vapor mole fraction, hydrogen mole fraction

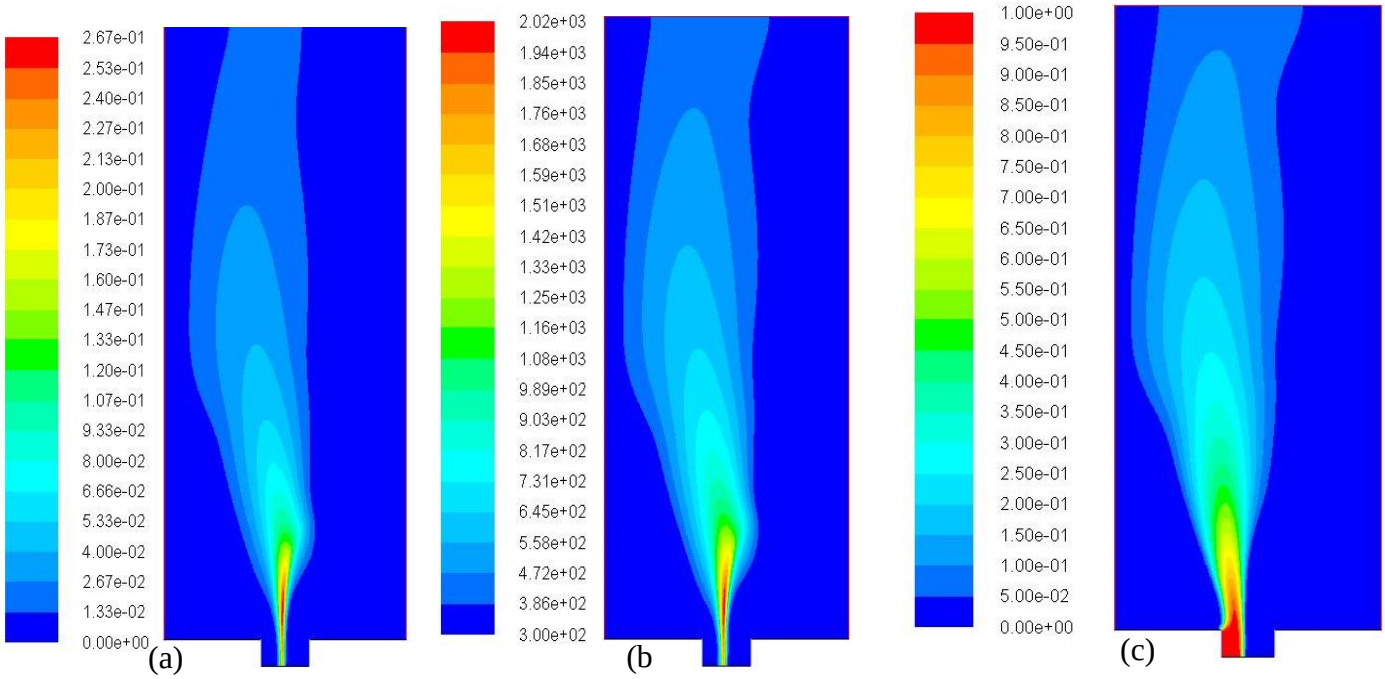

Figure 10 Isocontours of (a) H_2O mole fraction, (b) Temperature, and (c) H_2 mole fraction at the plane of symmetry.

and temperature at the plane of symmetry. It is seen that the flame is located in the stagnation plane (mid-plane between the two jets) then it shift slightly on the oxidizer side relative to the stagnation plane, whereas farther away from the axis, it curves to the fuel side; the curvature becomes more pronounced close to the boundary of the nozzles. This asymmetry is due to the high diffusivity and viscosity of hydrogen, the difference in thermal diffusivities of the fuel and oxidizer streams, and the slight density difference of the two jets.

Figure 11 and 12 show the velocity vectors and the velocity contours at the plane of symmetry. It can be seen clearly that the maximum velocity is located in the in stagnation plane between the two jets.

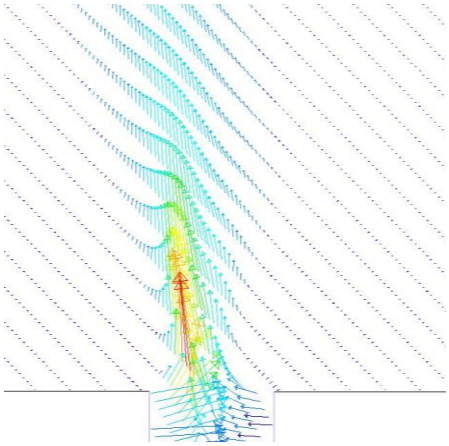

Figure 11 Velocity vectors at the plane of symmetry.

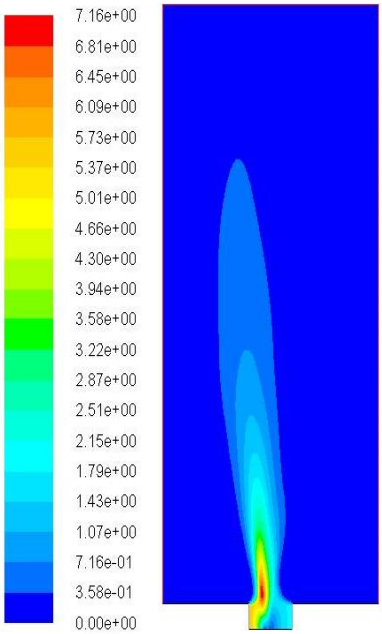

Figure 12 velocity contours at the plane of symmetry.

The temperature, velocity, water vapor and hydrogen mole fraction profiles at the stagnation plane are presented in Figure 13. The maximum value of the temperature is found to be about

1830 K. the high value could be due to the chemistry model that is used in the current study.

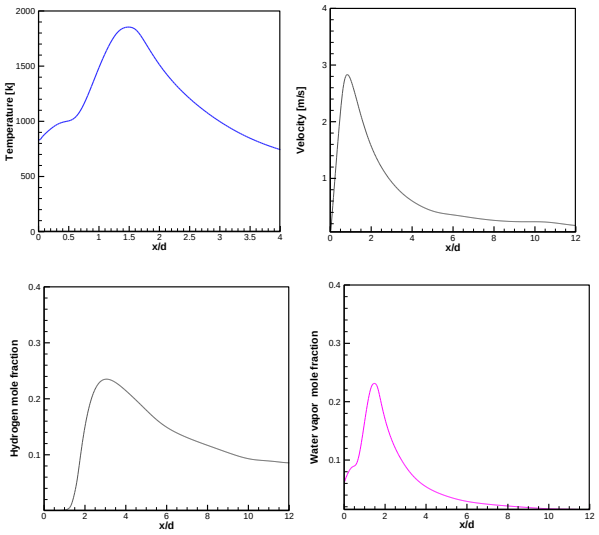

Figure 13 Profiles of temperature, velocity, water vapor and hydrogen mole fraction at the stagnation plane.

CONCLUSION

Numerical study is conducted to investigate the flowfield characteristics of turbulent opposed jets. Unconfined and confined boundary conditions are used and examined. Flowfields are obtained for different jet ratios. For air-air case, stagnation zone is formed in the middle for the JR =1 and moved towards the weaker jet when JR is less than 1. Confined boundary condition shows variation in flowfields due to presense of wall but this effect becomes week when JR is less than 0.53. Results for reacting flows of hydrogen-air flames that the flame is located in the stagnation plane, the mid-plane between the two jets, then it shift slightly on the oxidizer side.

References

[1] C.K. Law, D.L. Zhu, G. Yu, Propagation and extinction of stretched premixed flames, in: Proceedings of the Combustion Institute, vol. 21, The Combustion Institute, 1986, pp. 1419–1426.

[2] R.J. Kee, J.A. Miller, G.H. Evans, G. Dixon-Lewis, A computational model of the structure and extinction of strained, opposed flow, premixed methane–air flames, in: Proceedings of the Combustion Institute, vol. 22, The Combustion Institute, 1988, pp. 1479–1494.

[3] M. Nishioka, S. Nakagawa, Y. Ishikawa, T. Takeno, NO emission characteristics of methane–air double flame, Combust. Flame 98 (1994) 127–138.

[4] Chou C., Chen J., Janicka J., Mastorakos E., Modeling of turbulent opposed-jet mixing flows with k-ε model and second-order closure, International Journal of Heat and Mass Transfer, 47,2004, pp 1023–1035

[5] Hosseinalipour, S.M., and Mujumdar, A.S., "Flow and Thermal Characteristics of Steady Two Dimensional Confined Laminar Opposing Jets: Part I. Equal Jets," Int. Comm. Heat Mass Transfer, Vol. 24, No. 1, pp. 27-38, 1997.

[6] Eckstein et al.,"Modeling Of Turbulent Mixing In Opposed Jet Configuration: One-Dimensional Monte Carlo Probability Density Function Simulation," Proceedings of the Combustion Institute, Volume 28, 2000/pp. 141–148.

[7] Jones, W. P., and Prasetyo, Y., *Proc. Combust. Inst.* 26:275–282 (1996).

[8] Mastorakos, E., Taylor, A. M. K. P., and Whitelaw, J. H., *Combust. Flame* 91:55–64 . (1992).

[9] Kistler, J. S., Sung, C. J., Kreutz, T. G., Law, C. K., and Nishioka, M., *Proc. Combust. Inst.* 26:113–120 (1996).

[10] Im, H. G., Chen, J. H., and Chen, J.-Y., *Combust. Flame* 118:204–212 (1999).

[11] Frouzakis et al., **"**From Diffusion to Premixed Flames in an H2/Air Opposed-Jet Burner: The Role of Edge Flames," *Combustion And Flame* 130:171–184 (2002).

[12] Weifeng et al.,"Experimental and numerical study on stagnation point offset of turbulent opposed jets," Chemical Engineering Journal 138 (2008) 283–294.

[13] ANSYS Fluent 14.5 User's Guide , 2013.

[14] Wilcox, D. C., 1998, Turbulence Modeling for CFD, DCW Industries Incorporation.

[15] Launder, B. E., and Spalding, D. B., 1972, Lectures in Mathematical Models of Turbulence, Academic Press, London, England.

[16] Frouzakis C., Lee J., Tomboulides A., and Boulouchos K., Two-dimensional direct numerical simulation of opposed-jet hydrogen-air diffusion flame, Twenty-Seventh Symposium (International) on Combustion/The Combustion Institute, 1998, pp. 571–577